# Terahertz emission of atoms driven by ultrashort laser pulses

Zhaoyan Zhou, Dongwen Zhang, Zengxiu Zhao, and Jianmin Yuan*
*Department of Physics, National University of Defense Technology, Changsha 410073, People's Republic of China*
(Received 5 August 2008; revised manuscript received 9 March 2009; published 24 June 2009)

Terahertz (THz) emissions of an isolated atom in an ultrashort (100 fs) laser field are simulated by solving the time-dependent Schrödinger equation. From numerical calculations with one- and three-dimensional hydrogen atom models and a short-range shallow potential model, it can be concluded that continuum THz emissions occur more readily following transitions involving intermediate states above rather than those well below the ionization threshold of the system. Line-shaped THz emissions from transitions between high-lying Rydberg states are also found. The models are also used to describe the observed enhanced terahertz emissions with a superposed second-order harmonic laser field or a spatially constant electric field. The dependence of the THz field strength on the intensities of the fundamental laser field and the superposed field is also examined. Strong field approximation is extended to analyze the general features of THz emissions resulting from continuum free-free transitions of an electron in strong laser fields. These calculations contribute to an understanding of the THz emission processes when strong laser fields interact with atomic and molecular systems that have larger ionization potentials and where multiphoton processes are involved in order to generate THz emissions effectively.

DOI: 10.1103/PhysRevA.79.063413 PACS number(s): 32.80.Rm, 42.50.Hz, 42.65.Ky

## I. INTRODUCTION

During the last decade, the generation and detection of terahertz (THz) electromagnetic pulses have raised much interest because of applications such as rapid THz imaging, nonlinear THz spectroscopy, and chemical identification. Physical processes responsible for THz emissions have been studied extensively and most of the studies have been designed around a classical model, namely, that transient electric currents are responsible for THz radiation both for laser-induced plasmas [1–8] and laser-semiconductor interactions [9–14]. Electric current density is often interpreted macroscopically in terms of the velocity [4,9,15,16] or density [17] of all electrons together. In these previous studies, THz emission is interpreted in terms of optical rectification and instantaneous polarization [18,19], the ionization induced plasma oscillations [20,21], and asymmetrical double quantum wells [22,23]. Although the details of the explanations differ, it is generally accepted that a system with a broken symmetry is capable of creating a coherent wave packet thereby strengthening the THz emissions. The asymmetry can be achieved by using a nonlinear medium lacking inversion symmetry or by using an asymmetrical laser pulse. $LiNbO_3$, $LiTzO_3$ [24], organic crystal DAST [25,26] and GaAs and ZnTe [27,28] are the nonlinear media most commonly used and their activities in a laser field have usually been described using second-order polarization [12,14,27]. The amplitude and frequency of the emitted THz electromagnetic pulses are determined by the parameters of the laser pulse and the properties of the nonlinear medium. The asymmetrical laser fields most commonly used include an optical ac bias achieved by superposing a second-order harmonic laser field [1–4,6,7], an externally applied dc bias [5,9–11,29], or an ultrashort laser pulse [17]. It has also been widely accepted that ionizations are essential for the THz emissions from laser-excited gases since Hamster *et al.* [30] first demonstrated that THz emissions from noble gases were subsequent to the ionization caused by intense laser fields.

The basic physical processes responsible for radiative emissions are electron transitions between the electronic energy levels directly or via intermediate states. When multiphotons are involved in transition processes, such as a multiphoton ionization process of an atom in strong laser fields [20,21,30], many intermediate states are usually involved. This kind of nonlinear process is difficult to describe in terms of second-order and higher-order nonlinear polarization parameters, which have often been used in the past to describe the parametric conversion from laser field to THz emissions.

This study examines the THz emission from an isolated atom in an ultrashort (100 fs) laser pulse from a quantum-mechanical perspective by solving the time-dependent Schrödinger equation (TDSE). THz emissions with different laser intensities have been explained relative to electron activities in atomic systems. Other nonlinear phenomena such as high-order harmonic generation (HHG) and above-threshold ionization (ATI), along with the interaction between intense laser pulses and atoms, have been included to clarify the generation processes of THz emissions and the correlations between the THz emissions and HHG. An atomic hydrogen model is used to simulate the THz emissions from intense ultrashort laser ionized gases, and an electron in a short-range shallow potential model is used to simulate the THz emissions of the semiconductor systems irradiated by less intense laser pulses. Although the TDSE approach has been used widely for upward parametric conversions generating HHGs, no evidence has been found that this approach has been used in relation to downward parametric conversions of THz emissions. The results of this study, such as the calculated relationship between the THz field strength and the THz wave bandwidth on the intensity and pulse width of the incident laser field, compare favorably

*Corresponding author: jmyuan@nudt.edu.cn

 

to previous studies and the corresponding explanations using the macroscopical nonlinear effects when the laser intensity is not too high, although the effects of environment and propagation are excluded.

Discussion of the findings centers around the superposing of a second-order harmonic laser field and application of an external dc bias. Section II of this report comprises a general description of the methods for solving the TDSE of an atom in a laser field. Section III explains the transition processes involved in the generation of THz emissions from the perspective of the atomic hydrogen model. Section IV shows the calculations for the mixing of fundamental and second-order harmonic laser fields for both atomic hydrogen and short-range potential models so that THz generation is enriched. In Sec. V THz emissions resulting from the optical transitions between continuum states of an electron in strong laser fields are explained by quantum theory of strong field approximation, and finally, in Sec. VI, some other results relating to dc electric bias have been included.

## II. THEORETICAL FRAMEWORK

The methods for solving the TDSE are based on the numerical solution of the TDSE [in atomic units (a.u.)] on a set of discrete grids,

$$i\frac{\partial}{\partial t}\psi(\mathbf{r},t) = (\hat{H}_0 + \hat{H}_I)\psi(\mathbf{r},t), \tag{1}$$

where $\hat{H}_0$ is the field-free Hamiltonian and $\hat{H}_I$ is the interaction part given in dipole approximation,

$$\hat{H}_I = -\mathbf{E}\cdot\mathbf{r}f(t)\cos(\omega t). \tag{2}$$

Throughout this study, a Gaussian-enveloped laser pulse and linearly polarized laser field is used. The split-operator method [31,32] is used to derive the wave function from Eq. (1). Numerical integrations are carried out at time intervals of 0.2 a.u. and grid spaces of 0.2 a.u. resulting in a convergence of better than $10^{-2}$ for the relative changes in calculated spectra in the THz region when the intervals are halved. The expression in momentum space can be easily computed for the split-operator method, which is realized by the mutual conversion of the wave function between coordinate and momentum spaces. Once the wave function is determined, the induced dipole moment can be computed. Thus, in a one-dimensional (1D) calculation, the dipole moment in length, velocity, and acceleration forms can be expressed as

$$d_L(t) = \langle\psi(x,t)|x|\psi(x,t)\rangle, \tag{3}$$

$$d_V(t) = \langle\psi(p,t)|p|\psi(p,t)\rangle, \tag{4}$$

$$d_A(t) = \langle\psi(x,t)|\frac{\partial V(x)}{\partial x}|\psi(x,t)\rangle + E_L f(t)\cos(\omega t)\langle\psi(x,t)|\psi(x,t)\rangle. \tag{5}$$

The corresponding emission amplitude spectrum is obtained from the Fourier transformation of the time-dependent dipole moment:

$$P_L(\omega) = \left|\frac{\omega^2}{t_f - t_i}\int_{t_i}^{t_f} d_L(t)e^{-i\omega t}dt\right|, \tag{6}$$

$$P_V(\omega) = \left|\frac{\omega}{t_f - t_i}\int_{t_i}^{t_f} d_V(t)e^{-i\omega t}dt\right|, \tag{7}$$

$$P_A(\omega) = \left|\frac{1}{t_f - t_i}\int_{t_i}^{t_f} d_A(t)e^{-i\omega t dt}\right|. \tag{8}$$

It has been shown that these three dipole forms, Eqs. (6)–(8), are generally not equal to each other, even for an exact wave function [33–35]. The equality happens only when the dipole moment and its time derivative at the end of the pulse are zero, which does not occur when substantial ionization takes place. The length form of the dipole moment requires distance from the nucleus while acceleration form requires close proximity of the wave function to the nucleus. Accurate determination of the wave function, however, is difficult distant from the nucleus due to the reflection of the wave function from the integration edge, and difficult very close to the nucleus due to the depth of the potential well. Velocity form does not appear to suffer the same constraints so, unless otherwise specified, the numerical results have been obtained with the velocity form. The size of the numerical integration is restricted to $|x|=3200$ a.u.. A smooth cosine mask function [36] is applied from $|x|=200$ a.u. to the edges of the grids to reduce the influence of the reflected wave function from the numerical integration edges. Thus, the norm of the wave function is not conserved and the electron density removed by the mask function is treated as ionization while the decrease in the norm is considered to be the probability of ionization.

Three-dimensional (3D) calculations are also made for the true hydrogen atom with the total wave function being expanded in terms of the Legendre polynomials in the $(r,\theta)$ coordinates [37] as

$$\psi(r_i,x_j,t) = \sum_{l=0}^{L}\frac{1}{r}f_l(r_i,t)P_l(x_j), x_j = \cos\,\theta_j, \tag{9}$$

and the split-operator method is applied only on the terms of $f_l$. The dipole velocity is expressed in the form

$$d_V(t) = \langle\psi(\mathbf{p},t)|p_z|\psi(\mathbf{p},t)\rangle, \tag{10}$$

where $z$ is the linear polarization direction of the laser field. Considering the expansion in Eq. (9) and the characteristics of the Legendre polynomials, one can find

$$\begin{aligned} d_V(t) &= \sum_{l=0}^{L-1} d_{Vl}(t) \\ &= \sum_{l=0}^{L-1} C_l[\langle f_l(p,t)|p|f_{l+1}(p,t)\rangle + \langle f_{l+1}(p,t)|p|f_l(p,t)\rangle], \end{aligned} \tag{11}$$

where $C_l$ is the coupling constant and has the form

$$C_l = \frac{2(l+1)}{(2l+1)(2l+3)}. \tag{12}$$

Thus, only the transitions between different angular states with $\Delta l = \pm 1$ are able to take place and we can calculate each spectrum produced by transitions between $l$ and $l+1$ separately from the single $d_{Vl}(t)$,

$$P_{Vl}(\omega) = \left| \frac{\omega}{t_f - t_i} \int_{t_i}^{t_f} d_{Vl}(t) e^{-i\omega t} dt \right|. \tag{13}$$

These different components $P_{Vl}(\omega)$ are often called partial dipole contributions[35].

## III. THZ EMISSION IN A ONE-COMPONENT LASER PULSE

The accuracy of the numerical calculations is examined before looking at the dependence of the THz emission on the ionization potential of the emitting atom using calculations based on a one-dimensional soft Coulomb potential model [38]. This in turn, together with a three-dimensional calculation, leads to a clarification of which transitions contribute most to the THz emissions from an atomic system,

$$V(x) = -\frac{1}{\sqrt{(x^2 + a)}}. \tag{14}$$

This potential is widely used because it eliminates the singularity of the Coulomb potential at the origin by the parameter $a$ and can simulate the reaction of the true atom under linearly polarized laser pulse well. $a=2.0$ is chosen throughout this paper unless specially stressed, with the ionization potential equal to that of the true hydrogen atom, 13.6 eV. The Gaussian-enveloped laser field with 40 optical cycles (o.c.), 106 fs full width at half maximum (FWHM) pulse width, $1.26\times10^{14}$ W/cm$^2$ intensity, and 800 nm wavelength is adopted. In order to get an adequate frequency resolution in the THz range, we take the calculations extended to about 5.3 ps (2000 o.c.), in other words, the evolution of the state continues even the laser pulse has been passed over. Then the finest calculated spectrum resolution is about 0.188 THz.

In order to examine the accuracy of the numerical integration, the calculated spectra for length, velocity, and acceleration forms are compared (see Fig. 1). In Fig. 1, the amplitude of the THz emissions for the length form is highest because of the influence of the reflections, while the acceleration result is slightly lower than the other two expressions and is found to be unreliable for very low frequencies. As mentioned previously in relation to Eqs. (6)–(8), equality of the three forms requires both the dipole moment and its time derivative to be zero at the end of the laser pulse. Compared to the spectra in the HHG region, agreement between the THz spectra calculated with three different forms is more sensitive for the nonzero residual dipole moment and its time derivative after the laser pulse. About 95% of ionizations is predicted following the laser pulse given in Fig. 1.

Thus, the results throughout this report have been expressed in terms of the velocity form and have been converged for the different numerical grids. In Fig. 1, apart from

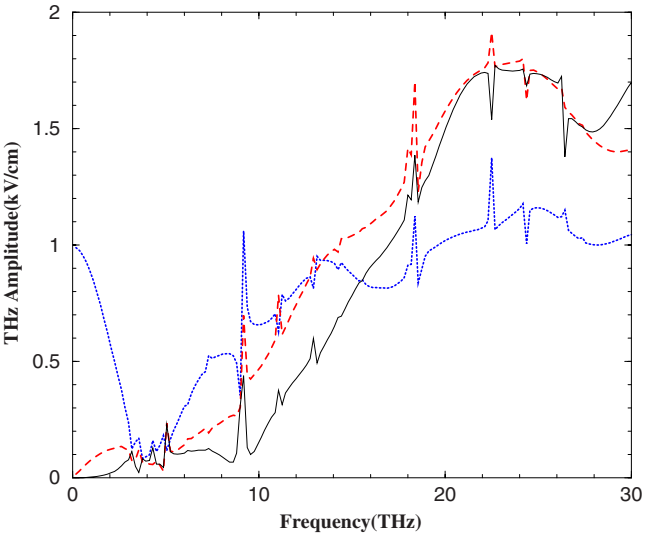


FIG. 1. (Color online) The THz spectrum for the soft Coulomb potential $V(x) = -1/\sqrt{x^2+2}$ represented in length (solid line), velocity (dashed line), and acceleration (dotted line) form. The laser pulse has intensity of $1.26\times10^{14}$ W/cm$^2$, wavelength of 800 nm, and is Gaussian-enveloped with 106 fs (FWHM) pulse width.

the strong continuum THz emissions, many sharp peaks corresponding to the transitions between the high-lying Rydberg states are observed. The energy differences between these states are small enough to fit in the THz range. The Fano-type shape of these lines may have been due to the interference between the resonant transitions and the continuum background. No matter what parameters of the laser pulse are chosen or what dipole moment forms are used, these peaks appear at the same places for the same atomic system. These lines also provide information about the energy levels of the atomic system and the dynamics of the atomic state population under the laser field. The lowest 20 eigenvalues and the energy differences between adjacent eigenstates calculated with the same numerical method are displayed in Table I. The differences are expressed in THz units for easy comparison with the sharp lines seen in Fig. 1. The positions of these lines correspond to the energy differences between proper eigenstates with different parities. The following section provides more details of how these sharp structures are produced mainly after the laser pulse or more specifically that they ensue from the automatic radiative transitions after a prepopulation of the high Rydberg states created by laser pulses and that their positions are not influenced by the laser fields.

Ionization potential is critical to THz emission output. The larger the ionization potential, the more photons are needed to excite an electron to the continuum states, and for the same degree of excitation, a more intense laser field is needed. The ionization potential can be changed by taking different $a$ values for the soft Coulomb potential. For $a=0.4$, 1.0, and 2.0, ionization potentials of 26.5, 18.2 and 13.6 eV, respectively are taken. As shown in Fig. 2, without changes in the laser pulse, the THz amplitude is found to be inversely proportional to the strength of the attractive potential or the ionization potential of the atom. This is similar to

TABLE I. Energy (in a.u.) of the first 20 low-lying eigenstates of the 1D soft Coulomb potential $V(x)=-1/\sqrt{x^2+2}$ and the energy differences between the adjacent eigenstates (in THz).

| $n$ | $E_n$ (a.u.) | $E_n-E_{n-1}$ (THz) |
|---|---|---|
| 0 | −0.50000862 | |
| 1 | −0.23291542 | 1757.19216092 |
| 2 | −0.13383829 | 651.82324435 |
| 3 | −0.08478435 | 322.72333773 |
| 4 | −0.05886173 | 170.54351345 |
| 5 | −0.04282168 | 105.52666122 |
| 6 | −0.03274307 | 66.30666420 |
| 7 | −0.02568301 | 46.44778893 |
| 8 | −0.02078605 | 32.21679210 |
| 9 | −0.01708453 | 24.35214941 |
| 10 | −0.01435002 | 17.99017990 |
| 11 | −0.01217497 | 14.30959096 |
| 12 | −0.01049664 | 11.04160341 |
| 13 | −0.00911217 | 9.10835353 |
| 14 | −0.00800935 | 7.25541300 |
| 15 | −0.00707445 | 6.15063161 |
| 16 | −0.00631147 | 5.01965417 |
| 17 | −0.00565080 | 4.34645890 |
| 18 | −0.00510123 | 3.61560107 |
| 19 | −0.00461724 | 3.18416687 |

the results of previous experiments, which generate THz pulses from noble gases [1]. Excitations of the atomic system to states above the ionization threshold also play an important role in the THz emissions. With the same laser pulse, the lower the ionization potential, the greater the possibility of an electron will be excited to the continuum states. Since optical transitions among continuum and high Rydberg states

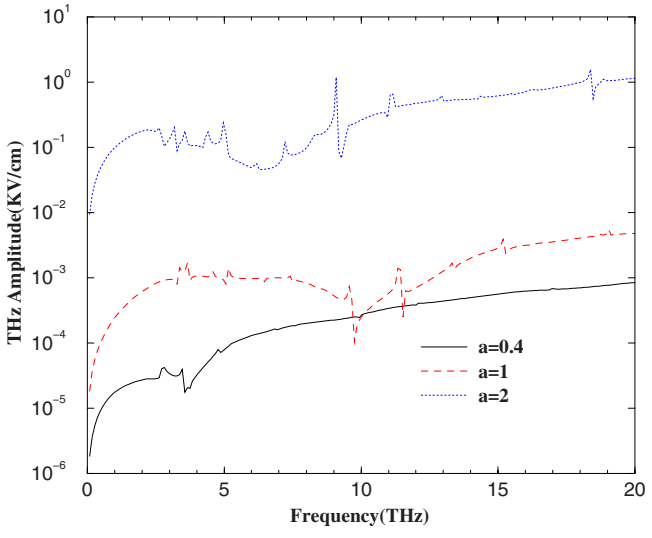


FIG. 2. (Color online) The velocity form of THz spectrum for the soft Coulomb potential $V(x)=-1/\sqrt{x^2+a}$ with $a=0.4$, 1.0, and 2.0, respectively. The laser field is the same as that in Fig. 1.

are the main processes to generate THz range emissions, in order to increase the frequency of these kinds of transitions, an adequate driving laser pulse is required to create many repeated loops of excitation from an initial bound state to the continuum state, followed by optically transiting nearby states to emit THz range photons, before finally recombining the parent ion core with emission of a high order harmonic photon. It should be pointed out that with laser fields that are too strong, the electrons are likely to escape from the emitter resulting in the reduction in THz as well as HHG emissions.

Calculations of the three-dimensional Coulomb potential $V(\mathbf{r})=-\frac{1}{r}$ are made, as is an examination of the partial dipole contributions from transitions between different angular momentum states in this model. Figure 3 shows the HHG spectrum of the partial dipole contributions between $l=0,1$, $l=1,2$, $l=3,4$ states as well as values for the total spectrum. HHG has often been described as comprising three steps [39,40]: an electron is first ionized by a laser field and then accelerated in the field; when the direction of the laser field is reversed, the electron can be driven back to its parent ion; it recombines to the ground state, emitting its energy as one harmonic photon. As demonstrated by Chen *et al.* [35], the $l=0,1$ partial contribution accounts for the total harmonic spectrum within the plateau region while other partial dipole contributions are lowered by several orders compared with the total. This reinforces the notion that HHG is dominated by transitions ending in the ground state ($l=0$). The THz emissions seen in the total spectrum denoted in Fig. 3(a) are not obvious for the partial dipole contributions shown in Figs. 3(b)–3(d). Thus, the process of recombining to the bound state, which is necessary for HHG, does not contribute to the generation of THz emissions. Only the first two steps in the three-step process produce THz emissions. The total wave functions in terms of 82 Legendre polynomials, namely, $L=81$ in Eq. (9), are made; however, only calculations of 1000 o.c. are made to prevent divergence of the results. The results of the three-dimensional calculations are similar to the one-dimensional ones but much more time consuming so only one-dimensional model simulations have been included in subsequent discussions.

To distinguish the relative contributions of the radiative transitions among the continuum intermediate states of THz range emissions, the time-dependent dipole moment is derived from the calculated wave function when the bound state components have been subtracted. More specifically, the dipole moment is calculated from $d_V(t)=\langle\psi_c(p,t)|p|\psi_c(p,t)\rangle$, where $\psi_c$ represents the continuum states. The corresponding spectrum is illustrated in Fig. 4(b) and the whole wave function spectrum is shown in Fig. 4(a). According to the three-step model for HHG spectra, recombining of the returning electron to the ground state is essential for HHG emissions. Thus, the HHG peaks cannot be seen clearly when the bound state components are subtracted. The spectra in the THz emission range [the insets in Figs. 4(a) and 4(b)] coincide closely for the two cases, not withstanding the lack of transitions between the high Rydberg states as they cannot exist without bound Rydberg states. The bound state components are subtracted only in the dipole moment calculation and not in the process of solving the TDSE, so this should not be viewed a source of error in the above

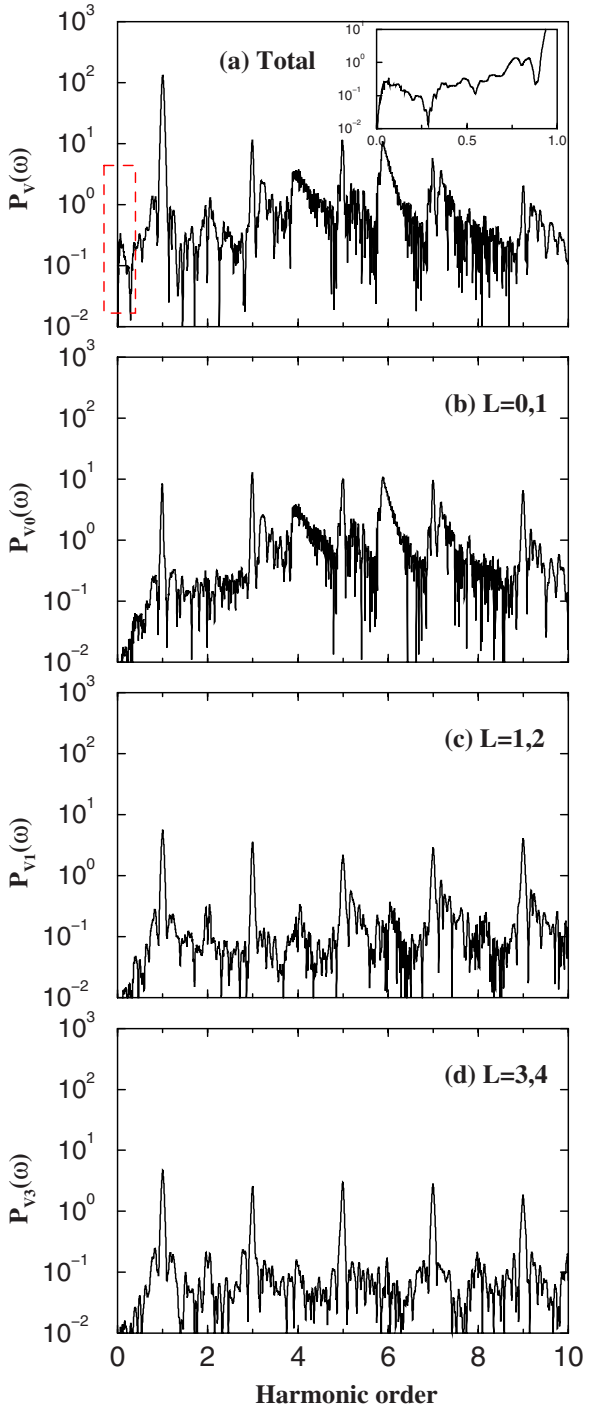


FIG. 3. (Color online) (a) HHG spectrum of the 3D Coulomb potential under the same laser pulse as Fig. 1. The partial dipole contributions from the dipole transitions (b) $l=0,1$, (c) $l=1,2$, and (d) $l=3,4$.

analysis. Although the recombining to the bound state contributes little to THz emissions, the closed loop process is necessary during the laser pulse interaction in order to generate substantial THz emissions. In other words, if the electron escapes too quickly to complete the three-step loop, the THz emission can be very weak.

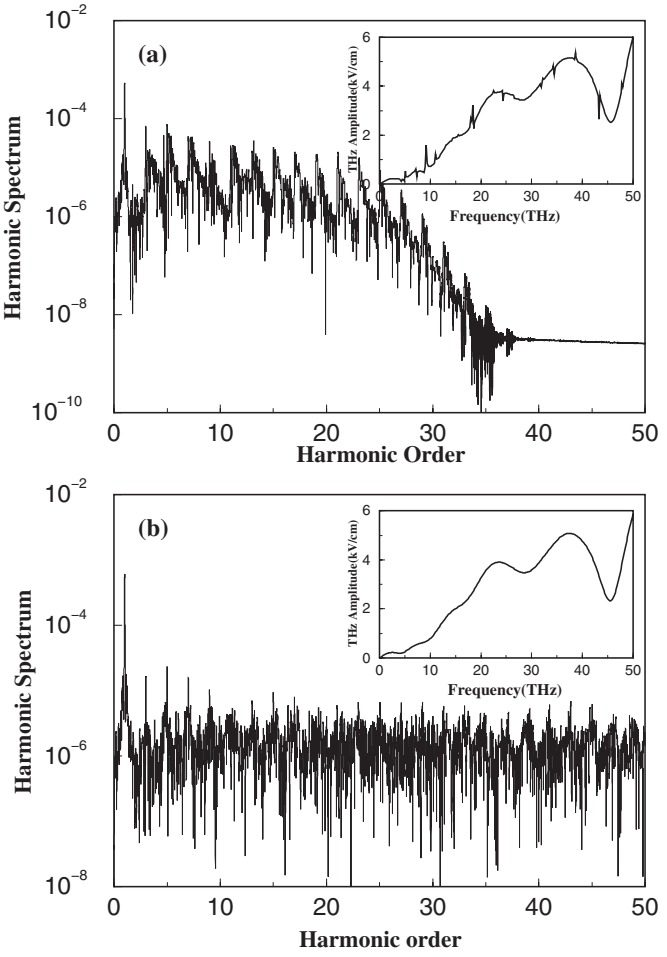


FIG. 4. The emission spectrum calculated from (a) the whole wave function and (b) part of the wave function including the continuum components only for the soft Coulomb potential $V(x)=-1/\sqrt{x^2+2}$. The spectrum in THz range is enlarged in the insets. The laser field is the same as that in Fig. 1.

## IV. WAVE MIXING PROCESS

In a recent study, enhanced THz emissions are observed when a fundamental and its corresponding second harmonic laser field are mixed [2]. The underlying mechanism is described as the "four-wave mixing" (FWM) process. The measured third-order nonlinearity ($\chi^{(3)}$) due to ponderomotive or thermal effects, however, is too small to explain the amplitude of the observed THz emissions in experiments [3]. Nonetheless, experiments involving plasma [6,7] and semiconductors [9] report THz amplitude scaling in terms of $\chi^{(3)}$, intensities of the fundamental and corresponding second harmonic laser fields, and their phase difference $\varphi$ [1–3,7,41]

$$E_{\mathrm{THz}} \propto \chi^{(3)}\sqrt{I_{2\omega}I_{\omega}}\cos\varphi. \tag{15}$$

This supports FWM as the principle mechanism for THz generation. The origin of $\chi^{(3)}$ is not addressed in these studies. The THz amplitude scaling premise is also demonstrated by the calculations herein revealing an amplitude comparable to previous experiments [4]. As shown in Fig. 5(a), the introduction of a $2\omega$ laser pulse with an intensity of 3.15

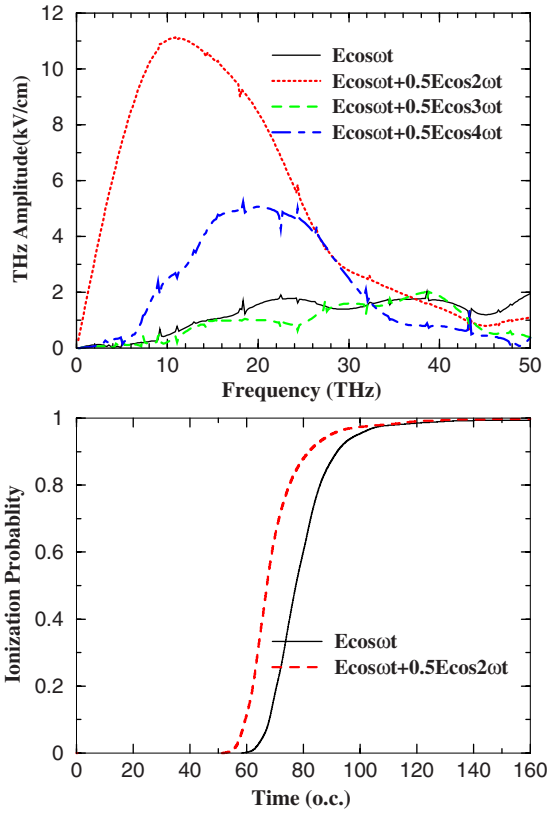


FIG. 5. (Color online) (a) The THz emission spectrum for the soft Coulomb potential in the mixing of the fundamental ($\omega$) and $n\omega$ laser fields whose intensity is a quarter of the fundamental one. The intensity of the fundamental laser field is $1.26\times10^{14}$ W/cm$^2$. (b) The corresponding ionization probability for the fundamental laser field and the mixing of the fundamental and its second harmonic laser fields.

$\times10^{13}$ W/cm$^2$ enhances the THz amplitude (about 11.14 kV/cm) by more than 1 order compared to one without. The calculated results for mixing of the fundamental laser field with a few higher-order harmonic fields are displayed in Fig. 5(a). The fundamental laser field does not change and the intensity of the second laser field is taken to be a quarter of the fundamental one. The presence of a $4\omega$ laser field can also increase THz emissions. When a minimum of six photons are involved in the THz emission loop the THz amplitude is found to be smaller than that for the corresponding four-photon loop in the $2\omega$ case. A laser field with a frequency of $3\omega$ does not work in accordance with parity conservation so it does not change the THz emissions substantially. This conclusion is consistent with the quantum interference theory [14,42–45], which relies on interference between one- and two-photon pathways among the continuum states of conduction and valence bands of the semiconductors. It is found that only the introduction of a $2n\omega$ laser field is able to open the quantum pathway of even photons.

To explore the detailed spectrum and the temporal THz emission process, a time-frequency analysis is performed by means of a wavelet transformation [40],

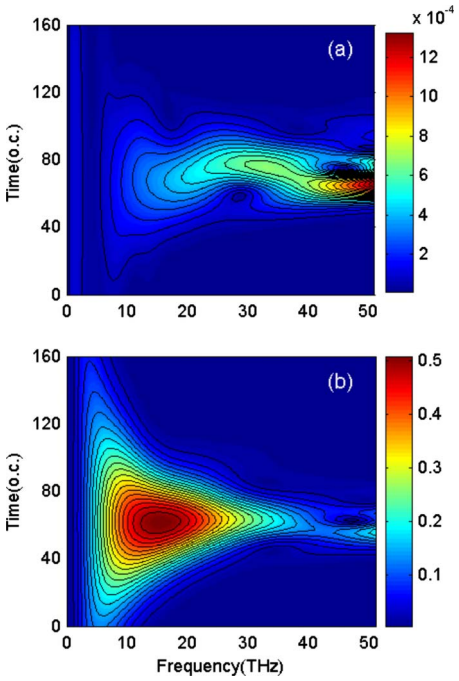


FIG. 6. (Color online) The 3D time-frequency spectra for the THz emissions under (a) the fundamental monochromatic laser field and (b) mixing of the fundamental and its second harmonic laser fields. The laser parameters are the same as those in Fig. 5.

$$A_\omega(t_0,\omega)=\int d(t)w_{t_0,\omega}(t)dt, \tag{16}$$

and

$$w_{t_0,\omega}(t)=\sqrt{\omega}W[\omega(t-t_0)], \tag{17}$$

where $W[x]=\frac{1}{\sqrt{\tau}}e^{ix}e^{-x^2/2\tau^2}$ to make the width of the time window increase with the decrease of frequency. In Eq. (16), $\tau$ set at 5 a.u. and $d(t)$ is adopted as the differential of the dipole velocity, which is equal to the dipole acceleration in this case. The result changes little when $\tau$ changes by around 5 a.u. Figure 6 shows the 3D time-frequency THz spectra for the soft Coulomb potential model with (a) the fundamental laser only and (b) mixing of the fundamental and its second harmonic laser field. The strength shown on the right of the figure indicates that with the introduction of $2\omega$ laser fields the THz emissions are much stronger and the intensity reaches its maximum at about 12 THz, which is consistent with the value displayed in Fig. 5(a). The THz emissions mainly occur from 40 to 80 o.c., which corresponds to the main period of time when ionization occurs. The corresponding time-dependent ionization probabilities for the two types of laser fields are shown in Fig. 5(b). This clarifies the time relationship between THz emissions and ionization. In the case of a one-component laser pulse, ionization occurs relatively slowly so the THz emission occurs later than that in mixed laser fields, as can be seen in Fig. 6(a). In both cases the THz emissions, except for the sharp lines due to the transitions among the Rydberg states, do not occur after the laser fields. This is in consistent with the conclusion in the

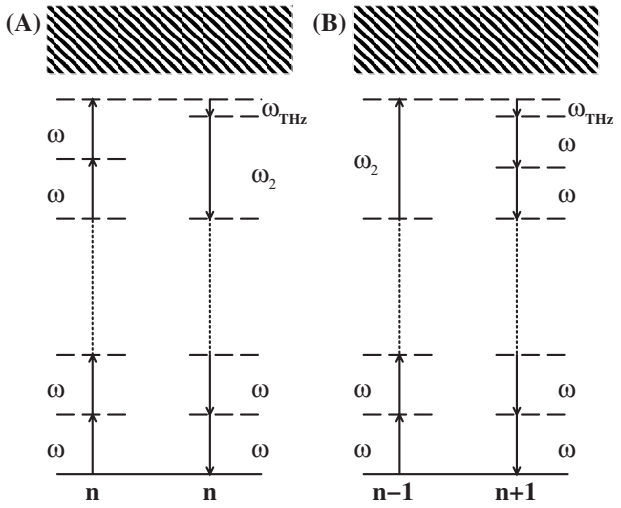


FIG. 7. Schematic diagrams of multiphoton transition processes of an atomic system to produce THz emissions. The intermediate levels are represented by the horizontal dashed lines and the continuum ionization levels of the atomic system are represented by the shadowed area. Starting from the same initial state (the ground state or an intermediate state), two typical processes are shown here: (a) two fundamental photons are absorbed and then one THz photon and a second harmonic photon are emitted; (b) one second harmonic photon is absorbed and then a THz photon and two fundamental photons are emitted.

previous section that the transitions among the continuum and high Rydberg states play an important role in the repeated loops of multiphoton optical excitation, THz emission, and radiative recombination when driven by a fundamental laser field and stimulated by its second harmonic laser field.

Compared to the periodic HHG emission characteristics following recollision of an electron with its parent ionic core driven by the laser fields [40], the wavelet transformation of THz emissions demonstrates a continuous change with time for a fixed frequency, namely, THz emissions occur in the whole acceleration process of electron in the laser fields, from a classical orbital point of view. Furthermore, the importance of transitions between the intermediate states lying within the continuum electron energy levels is demonstrated above. When viewed in combination, these features help to explain the observed enhancement of THz emissions following the mixing of the fundamental and second harmonic laser fields. Figure 7 shows how the bandwidth of the laser pulse affects THz emissions along two pathways. In pathway A, the system first absorbs $n(\geq 2)$ fundamental laser photons with an energy of $\hbar\omega$ and is then transmitted to an intermediate state. It then emits one photon with a frequency in the THz domain and a photon with an energy of about $2\hbar\omega$ before it finally comes back to the initial state. In pathway B, the system absorbs $n-2$ fundamental laser photons and one $2\hbar\omega$ photon and is then transmitted to an intermediate state. It then emits one THz photon and $n(\geq 2)\hbar\omega$ photons before it finally comes back to the initial state. In both pathways, the $2\omega$ photon's emission and absorption are stimulated by the second harmonic laser field. Transition via pathway A is also possible without this stimulation, but there would be less likelihood since second-order and other even-order harmonics are generally weaker than odd-order harmonics when produced by a fundamental laser only. A closed loop of transitions can also be completed with two THz photons without the second harmonic photons, but with much less likelihood. In this case, the system will absorb $n$ photons and emit $n$ photons or absorb $n-1$ photons and emit $n+1$ photons in compliance with the parity and energy conservation requirement. Other combinations of fundamental laser photons, second-order harmonic photons, and a THz photon may be possible to make a closed loop of transitions, however, the four-photon process for the mixing of the fundamental and its second harmonic laser fields is the primary generation mechanism of THz emissions when $n=2$, which is the most likely case if the laser field is not very high.

For most atomic systems, two infrared photons are insufficient to excite the system to an intermediate state in the continuum ionized levels of the atom so an intermediate state well below the ionization threshold is required for the four-photon process mentioned above. Intermediate levels above the ionization threshold can only be reached by absorbing a greater number of photons, which is what is observed in the intense laser fields seen in Fig. 5. Nevertheless, for many semiconductor systems, two infrared photons are sufficient to excite an electron from a valence band to a conduction band.

Using a model of an electron in a short-range shallow potential of the form [46,47]

$$V(x) = -c_1 e^{-x^2/c_2}, \tag{18}$$

a significant increase in the THz emissions produced through the four-photon process is demonstrated when the position of the intermediate state is moved across the ionization threshold. For a finite-range potential, the Rydberg series are replaced by a few bound states whose number decreases with the decreasing potential range or strength [48]. The parameters in Eq. (18) are set at $c_1=0.3$ and $c_2=1.202$. Only one bound state exists for this potential and the ionization energy is $I_p=2.428$ eV, thereby satisfying $\hbar\omega < I_p < 2\hbar\omega$. This level of ionization potential has often been used in simulating the semiconductor systems in previous studies [14,42,49,50] and is found to be convenient for simulating the quantum interference processes. In this study only the bound state provides an appropriate initial and final state in the four-photon process. The electron is easily ionized by the field with a frequency of $\omega$ (two-photon ionization) or $2\omega$ (one-photon ionization). The intensities of the laser fields are chosen so that more than four photon processes would yield negligible differences in the results.

To find an increase in the THz emissions when the position of the intermediate state crosses the ionization threshold, the potential parameter $c_1$ in Eq. (18) is changed from 0.17 to 0.4, which results in corresponding changes to the ionization energy $I_p$ from 0.969 to 3.7763 eV. The intensities of the fundamental (800 nm) and its second harmonic laser field are fixed at $3.51\times10^{10}$ W/cm$^2$ and $1.404\times10^{9}$ W/cm$^2$, respectively. The center photon energy of the fundamental 800 nm laser field is 1.55 eV and $\varepsilon$ is used to denote the ratio of $I_p/\hbar\omega$, which ranges from 0.625 to 2.436. Figure 8(a) shows

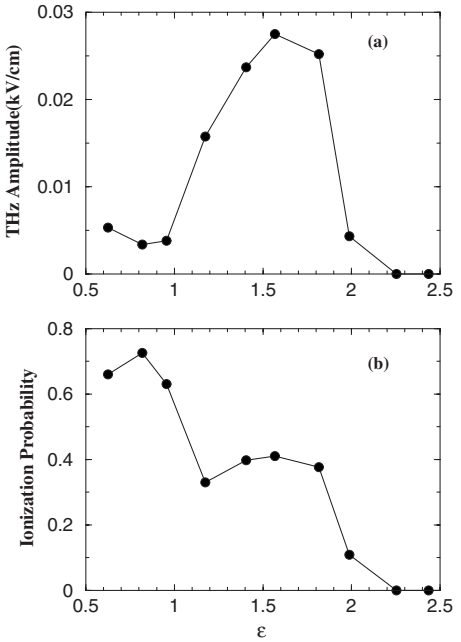


FIG. 8. (a) Dependence of THz field strength on $\varepsilon = I_p/\omega$, the ratio of the ionization potential $I_p$ to the center photon energy of the fundamental laser field. The intensities of the fundamental (800 nm) and its second harmonic are fixed at $3.51 \times 10^{10}$ W/cm$^2$ and $1.404 \times 10^9$ W/cm$^2$ for the short-range shallow potential $V(x) = -c_1 e^{-x^2/1.202}$. (b) The corresponding ionization probability for different $\varepsilon$.

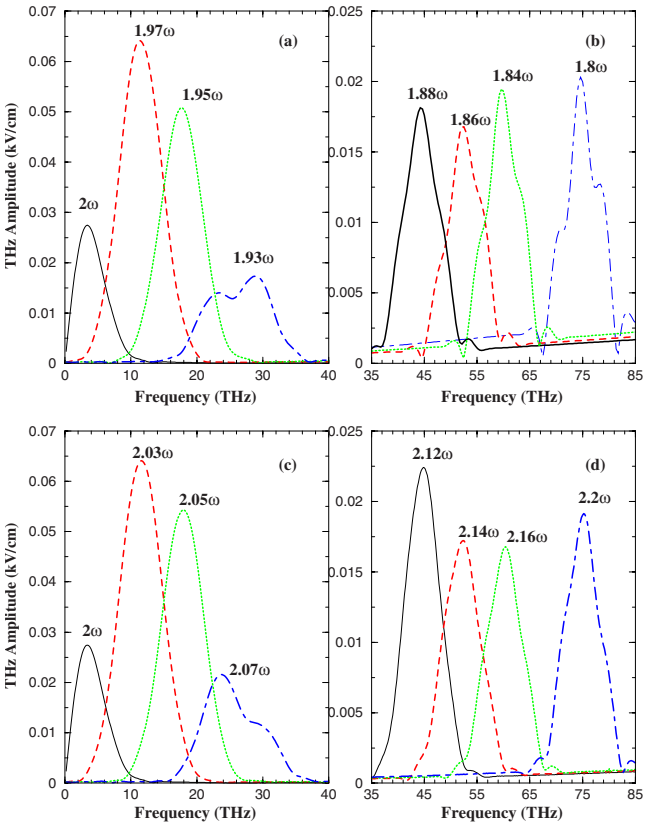


FIG. 9. (Color online) The THz emission spectrum of an electron in a short-range shallow potential model $V(x) = -0.3e^{-x^2/1.202}$ with the mixing of the fundamental laser field (800 nm, $3.51 \times 10^{10}$ W/cm$^2$) and the proximal second harmonic laser $\omega_2$ field ($1.404 \times 10^9$ W/cm$^2$). The frequency $\omega_2$ (denoted as a number times $\omega$ in the frame) ranges around $2\omega$, twice of the frequency of the fundamental laser pulse.

the dependence of the THz field amplitude on $\varepsilon$ with the corresponding ionization probability displayed in Fig. 8(b). Enhanced THz emissions can be seen in the $1.0 < \varepsilon < 2.0$ range, consistent with the condition of $\hbar\omega < I_p < 2\hbar\omega$ found necessary for enhanced THz emissions above. When $\varepsilon > 2.0$, two photons of the fundamental laser field are insufficient to excite the electron to an intermediate state above the ionization threshold. Then the four-photon process can only take place between the ground state and an intermediate state below the ionization threshold. It can be seen that there are almost no THz emissions in this case and the THz emissions are understood to be induced by virtual carriers, where the electrical transient results from a reactive current and is free from scattering effects [19]. This usually occurs at a much lower level than that induced by real carriers of the same laser field. The rapid decrease in excitation near or just below the band edge is also detected in experiments for GaAs samples [19] and is interpreted as the exponential decrease in optical absorption [51]. When $\varepsilon < 1.0$, one photon of the fundamental laser pulse is sufficient to excite the electron above the ionization threshold. The ionized electron is then less likely to absorb one photon than the bound electron and the closed four-photon loop is less likely to be completed than when $1.0 < \varepsilon < 2.0$. Moreover, the ionized electron is apt to be released because of the weak bond of the short-range potential and is also found to counter THz emissions. The turn-on effect is obvious when $\varepsilon > 1.0$.

The bandwidths of the THz spectra are also analyzed using the parametric potentials with $c_1 = 0.3$, $c_2 = 1.202$, and $I_p = 2.428$ eV. To show the dependence of the THz spectra on the second harmonic laser frequency, the second harmonic laser field is specified as a long flat-top envelope with a frequency of $\omega_2$ and varying around $2\omega$. This laser field remains constant throughout the calculations so its bandwidth can be omitted from analysis of the bandwidths of the THz spectra. The fundamental Gaussian-enveloped laser pulse, with a $\omega$ centered frequency and bandwidth (denoted as $\delta\omega$) of about 0.03 (1/o.c.) (11.25 THz) for the 106 fs (FWHM) Gaussian-enveloped pulse, does not change. Pathway A of the four-photon process mainly occurs when $\omega_2 < 2\omega$, which is denoted as $\omega_2 = 2\omega - \delta\omega_2$. Following the excitation that occurs from the absorption of two $\omega_1$ photons ($\omega - \delta\omega \leq \omega_1 \leq \omega + \delta\omega$) and emission of one $\omega_{\mathrm{THz}}$ photon, the electron recombines to the ground state by emitting a $\omega_2$ photon. Thus, the THz spectrum is broadened with higher $\delta\omega$, being the shorter duration of the fundamental laser pulse. Since the central $\omega$ photons are found to be the most likely ones absorbed by the electron, the THz spectra mainly center around $\omega_{\mathrm{THz}} = 2\omega - \omega_2$ for different values of $\omega_2$, as shown in Fig. 9(a). In this figure, the strength of the THz fields varies according to the different $\omega_2$ values. The strength is determined by the strength of the incident laser fields and the probability of absorbing or emitting photons. As the strength of the incident laser field remains constant for these calculations, the

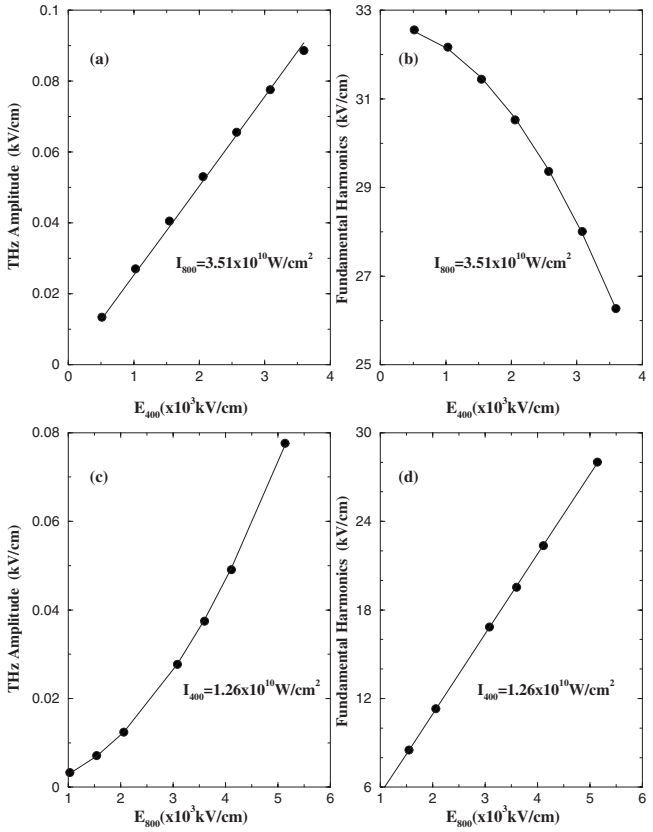


FIG. 10. Dependence of THz amplitude on (a) the amplitude of the $2\omega$ beam and (c) the amplitude of $\omega$ beam. Dependence of the fundamental harmonics amplitude on (b) the amplitude of the $2\omega$ beam and (d) the amplitude of $\omega$ beam. The solid lines are the linear and square fit and the dots are the calculated values for the short-range shallow potential model $V(x)=-0.3e^{-x^2/1.202}$.

probability of emitting $2\omega-\omega_2$ THz photon accounts for the strength of the THz emissions here. When the frequency of the THz emissions is high enough, this probability varies little and the strength of the THz field remains fixed at $2\omega-\omega_2$, as is shown in Fig. 9(b). Pathway B of the four-photon process mainly occurs when $\omega_2=2\omega+\delta\omega_2$ and the peaks of the THz spectra remain fixed at $\delta\omega_2$, as shown in Figs. 9(c) and 9(d). The THz emission behavior is similar to when $\omega_2=2\omega-\delta\omega_2$.

As mentioned previously, according to the four-photon process model involving superposed second harmonic laser fields over the fundamental one, the emission of THz photons can be attributed to the transitions between the continuum states referred to as the intermediate states. When $\omega_2=2\omega$, which pathway of A and B is the predominant case for the four-photon process relies on the relative intensities of the two incident laser fields. When different amplitudes of the $2\omega$ laser field are examined, the THz spectra are located in almost the same place. The dependence of the amplitudes of THz fields on the amplitude of the second-order harmonic laser fields, $E_{\mathrm{THz}}\propto E_{2\omega}$ as indicated in Eq. (15), is illustrated in Fig. 10(a). Two-photon excitation occurs mainly with higher intensities of the fundamental laser field. Two photons of the fundamental laser field are absorbed and one THz photon and one $2\omega$ are emitted when pathway A of four-photon process is followed. Thus, the amplitude of the fundamental harmonic reduces as $E_{2\omega}$ is increased and is found to be inversely proportional to the square of the amplitude of the second harmonic laser fields, as is shown in Fig. 10(b). In theory, the amplitude of the second-order harmonics evolves in the same manner as the THz emissions. As the second harmonic laser fields have a much longer duration than the THz emissions or the fundamental laser field, changes in the second harmonics are not obvious for the different intensities of the laser fields.

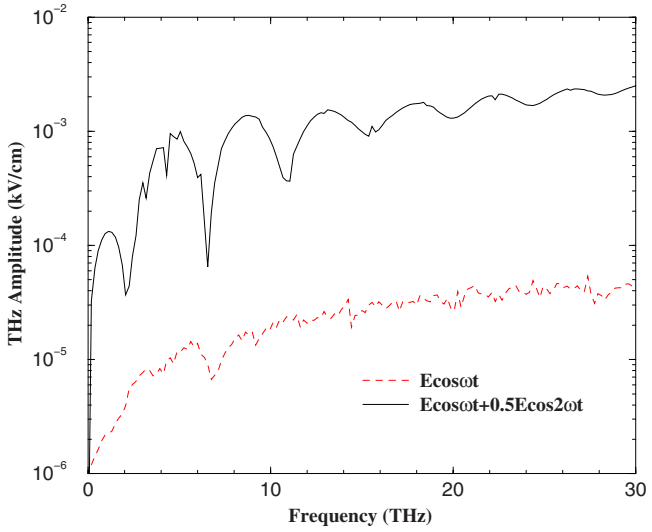


FIG. 11. (Color online) The THz emission spectrum calculated for the soft Coulomb potential $V(x)=-1/\sqrt{x^2+2}$ in the $3.51\times10^{12}$ W/cm$^2$, 800 nm laser field (dashed line) and the mixing of this fundamental and its second-order harmonic laser fields (solid line) whose intensity is a quarter of the fundamental one.

In contrast, when the intensity of the $2\omega$ laser field is higher, under the dominance of one photon excitation process the electron tends to absorb one photon of the second harmonic laser field and emit one THz photon and two photons of the fundamental laser field. With a fixed intensity of the $2\omega$ laser field, we find that $E_{\mathrm{THz}}\propto E_{\omega}^2$, as illustrated in Fig. 10(c). In the process of emitting one THz photon, two $\omega$ photons are also emitted and the amplitude of the fundamental harmonics changes in proportion to the amplitude of the fundamental laser field, as is shown in Fig. 10(d). This relationship between the THz field amplitude and the intensities of the two laser fields accords with the scaling law of Eq. (15) and is implicit in the four-photon process of generating THz emissions which involves two $\omega$ photons, one $2\omega$ photon, and one THz photon. Thus the amplitude of THz field is proportional to the amplitude of the $2\omega$ laser field and the square of the amplitude of the fundamental one. This relationship can be clearly seen in Fig. 10 where the intensity of the laser field is fixed so that multiphoton ($\geq$3) excitations can hardly happen.

THz intensity can also be strengthened under a 1D hydrogen model for the mixing of the fundamental and its second harmonic laser fields. Figure 11 shows the THz emission spectra when the intensities of the fundamental and its second harmonic laser fields are $3.51\times10^{12}$ W/cm$^2$ and $8.775\times10^{11}$ W/cm$^2$, respectively. There are almost no mul-

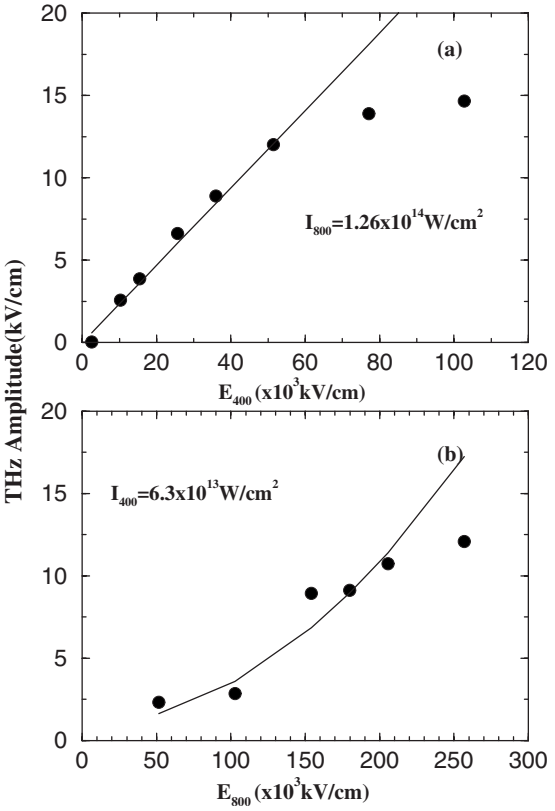


FIG. 12. Dependence of THz amplitude on (a) the amplitude of the $2\omega$ beam, (b) the amplitude of the $\omega$ beam. The solid lines are the linear and square fit and the dots are the values calculated for the soft Coulomb potential.

tiphoton excitations to the intermediate levels above the ionization threshold for this low intensity. The four-photon process can only occur between the ground state and intermediate levels well below the ionization threshold. Compared to the process without the second harmonic laser field, the THz emissions are strengthened as shown in Fig. 11; however, the magnitude is about 4 orders smaller than the values found in Fig. 5 where laser intensities are higher by only 2 orders. This result supports the argument above that THz emissions are more effectively produced by the transitions between the intermediate states above the ionization threshold.

More intense laser fields are also applied to examine their effects on the THz fields. The calculated results for the soft Coulomb potential model in Fig. 12 clearly show that the amplitude of the THz field is proportional to the amplitude of the second harmonic laser field. When the laser field is strong enough, saturation is reached and the scaling law becomes invalid due to the higher ionization probability and the lack of dominance of the four-photon process. With regard to the fundamental laser field, however, the relationship $E_{\mathrm{THz}} \propto I_{\omega}$ is not clear. This is attributed to the existence of many excited states below the ionization threshold and the need for more than two photons to excite the electrons to continuum states over the large ionization potential. More than eight photons from the fundamental laser pulse are needed to excite the electron from the ground state to an intermediate state above the ionization threshold and the fundamental laser field is also found to contribute to the escape of the electron. Thus the bound-bound and bound-free transitions in the soft Coulomb potential contravened the scaling law mentioned above and the dependence of THz fields on the intensity of the fundamental laser field cannot be clearly identified. This needs further investigation, so in the following section only the free-free transitions have been considered by means of the strong field approximations to simulate the four-photon process.

## V. FREE-FREE TRANSITIONS IN STRONG FIELD APPROXIMATION

As shown in Fig. 4, with only free-free transitions being included, the continuum THz emission spectra of an atom in strong laser field can be calculated very well. Therefore, the main features of the THz emission of an atom in strong laser field may be obtained using adequate analytic model of free electron in strong laser fields. The strong field approximation theory, which is extended here to calculate the THz emissions, is developed by Lewenstein *et al.* [52] to calculate the HHG. Under this theory, the time-dependent wave function is expanded in terms of the ground state and the continuum states; in other words, the contributions of all the excited bound states are ignored [53,54]. The continuum states are approximated by the Volkov states and the influence of atomic potential is neglected [53]. The amplitude of the electron being excited from the ground state to a continuum state by the laser field is given by

$$\mathbf{b}(\mathbf{v},t) = i\int_0^t dt' E(t') d_x[\mathbf{v}+\mathbf{A}(t)-\mathbf{A}(t')] \times \exp\left\{-i\int_{t'}^t \left[\frac{[\mathbf{v}+\mathbf{A}(t)-\mathbf{A}(t'')]^2}{2}+I_p\right]dt''\right\}, \tag{19}$$

where $\mathbf{d}(\mathbf{v})$ is the transition dipole moment from the ground state to the continuum state with momentum $\mathbf{v}$ and $d_x(\mathbf{v})$ is the component parallel to the polarization axis, which is chosen to be the $x$ axis. $\mathbf{A}(t)=[-E\sin(\omega t),0,0]$ and $E(t)=E\cos(\omega t)$ are the vector potential and the electric field of the laser field. If the canonical momentum $\mathbf{p}=\mathbf{v}+\mathbf{A}(t)$ is introduced, the amplitude can be rewritten as

$$\mathbf{b}(\mathbf{p},t) = i\int_0^t dt' E(t') d_x[\mathbf{p}-\mathbf{A}(t')] \times \exp\left\{-i\int_{t'}^t \left[\frac{[\mathbf{p}-\mathbf{A}(t'')]^2}{2}+I_p\right]dt''\right\}. \tag{20}$$

The strong field approximation theory is used here to examine the contributions of the free-free transitions to THz emissions. Note that the $x$ component of the dipole moment between two continuum states $|\mathbf{v}\rangle$ and $|\mathbf{v}'\rangle$ is given in length gauge by

$$\langle \mathbf{v}|x|\mathbf{v}'\rangle = i\nabla_{\mathbf{v}}\delta(\mathbf{v}-\mathbf{v}'). \tag{21}$$

Then the $x$ component of the integral dipole moment induced by the whole free-free transitions in the laser field is thus given in length gauge by

$$\begin{aligned} d_x(t) &= \int d\mathbf{v}\int d\mathbf{v}'\mathbf{b}_{\mathbf{v}}^*\langle \mathbf{v}|x|\mathbf{v}'\rangle\mathbf{b}_{\mathbf{v}}' \\ &= \int d\mathbf{v}\int d\mathbf{v}'\mathbf{b}_{\mathbf{v}}^* i\nabla_{\mathbf{v}}\delta(\mathbf{v}-\mathbf{v}')\mathbf{b}_{\mathbf{v}}' \\ &= i\int d\mathbf{v}\mathbf{b}_{\mathbf{v}}^*\frac{d\mathbf{b}_{\mathbf{v}}}{d\mathbf{v}}, \end{aligned} \tag{22}$$

where

$$\begin{aligned} \frac{d\mathbf{b}_{\mathbf{v}}}{d\mathbf{v}} &= \int_{t'}^{t} dt''[\mathbf{p}-\mathbf{A}(t'')]\int_0^t dt' E(t')d_x[\mathbf{p}-\mathbf{A}(t')]e^{-iS(t,t')} \\ &+ i\int_0^t dt' E(t')\nabla_{\mathbf{p}}d_x[\mathbf{p}-\mathbf{A}(t')]e^{-iS(t,t')}. \end{aligned} \tag{23}$$

For convenience, the following has been denoted $S(t,t') = \int_{t'}^{t}[\frac{[\mathbf{p}-\mathbf{A}(t'')]^2}{2}+I_p]dt''$. When the second term in Eq. (23) is neglected and Eqs. (19) and (23) are substituted into Eq. (22), the result is

$$\begin{aligned} d_x(t) = \int_0^t dt_1'\int_0^t dt_2'\int d\mathbf{p}\Bigg\{ & E(t_1')d_x[\mathbf{p}-\mathbf{A}(t_1')]E^*(t_2')d_x^* \\ & \times[\mathbf{p}-\mathbf{A}(t_2')]e^{-iS(t_2',t_1')}\int_{t_2'}^{t} dt''[\mathbf{p}-\mathbf{A}(t'')]\Bigg\} + \text{c.c.} \end{aligned} \tag{24}$$

The saddle-point method is then applied to the integration over momentum space. The saddle-point momentum is given by

$$p_{st} = \frac{x(t_2')-x(t_1')}{t_2'-t_1'}. \tag{25}$$

The equation is reduced to

$$\begin{aligned} d_x(t) = \int_0^t dt_1'\int_0^t dt_2'\Bigg\{ & \left(\frac{\pi}{\epsilon+i\tau/2}\right)^{3/2} E(t_1') \\ & \times d_x[p_{st}-A_x(t_1')]E^*(t_2')d_x^*[p_{st}-A_x(t_2')]\; e^{-iS(t_2',t_1')} \\ & \times\int_{t_2'}^{t} dt''[p_{st}-A_x(t'')]\Bigg\} + \text{c.c.}. \end{aligned} \tag{26}$$

Using a similar method, the $x$ component of the integral dipole moment in velocity form $d_v(t)$ can be defined by

$$\begin{aligned} d_v(t) = \int_0^t dt_1'\int_0^t dt_2'\Bigg\{ & \left(\frac{\pi}{\epsilon+i\tau/2}\right)^{3/2} E(t_1')d_x \\ & \times[p_{st}-A_x(t_1')]E^*(t_2')d_x^*[p_{st}-A_x(t_2')]e^{-iS(t_2',t_1')} \\ & \times[p_{st}-A_x(t)]\Bigg\} + \text{c.c.}. \end{aligned} \tag{27}$$

The only difference between Eqs. (26) and (27) is that the displacement $\int_{t_2'}^{t} dt''[p_{st}-A_x(t'')]$ in Eq. (26) is replaced by the momentum $p_{st}-A_x(t)$. As expected, the time differential of Eq. (26) is found to be an accurate reproduction of Eq. (27) for the length and velocity gauge relationships. The emission strengths calculated with Eqs. (26) and (27) relative to Eqs. (6) and (7), respectively, are almost the same. In Eq. (27), the term $p_{st}$ is related to the process of the electron born at $t_1$ jumping to another state at $t_2$ by the dipole transition under the influence of the laser field. The results obtained using this method are found to be in qualitative agreement with the numerical results. Further explanations will be given in the ensuing paragraphs.

The dependence of the THz amplitude on the intensities of the fundamental and its second harmonic laser fields and the phase differences between them, calculated with Eq. (27) for the hydrogen atom model, is illustrated in Fig. 13. The scaling law of Eq. (15) is evident in this case. The results further support the notion that free-free transitions are the main sources of THz emissions. The saturation phenomenon is not observed as electron depletion is not considered in this approximation.

The strength dependence of the THz field on the phase difference between the two lasers pulses $\varphi$ is explained by the change in the asymmetric laser field with $\varphi$ across an individual optical cycle [4], and in this case, the dependence can be associated with the ATI spectrum. It is proposed that in mixed laser fields the peak intensity, which means absorbing $2\hbar\omega$ photons in the continuum states of the ATI spectrum, as a function of the phase shift $\varphi$ is periodic and approximately proportional to cos $\varphi$ [55]. The tunneling of the electron in one optical cycle is seen to depend on the moment when the laser field reaches its peak value which is affected by the value of $\varphi$. This result is consistent with the mechanism for THz generation postulated herein and with the scaling law.

The strong field approximation results are found to be more regular than the results obtained from solving the TDSE. The center frequencies and widths of the THz spectra are found to be inversely proportional to the duration time of the laser pulses, as shown in Fig. 14(a). Since the continuum states in the numerical calculations are closely related to the potential model type, the emitted THz photon energy distribution is found to be different quantitatively to that of the strong field approximation. The TDSE results for the short-range potential model shown in Fig. 14(b) reveal that the frequency of the THz emissions also increases when the duration of the laser pulses is reduced, as in the case of the strong field approximation. Compared to the strong field approximation, however, there is a deviation of the inverse proportion due to the more complex continuum states. Consistent with our calculations, a previous study [6] shows that the center frequencies of the THz spectra decrease by increasing the length of the incident laser pulses. The frequency distributions of the THz emissions in the results of this study, however, differ quantitatively from those observed in the previous study, because of the greater complexity of true atoms, but as the generation mechanisms are the same, the

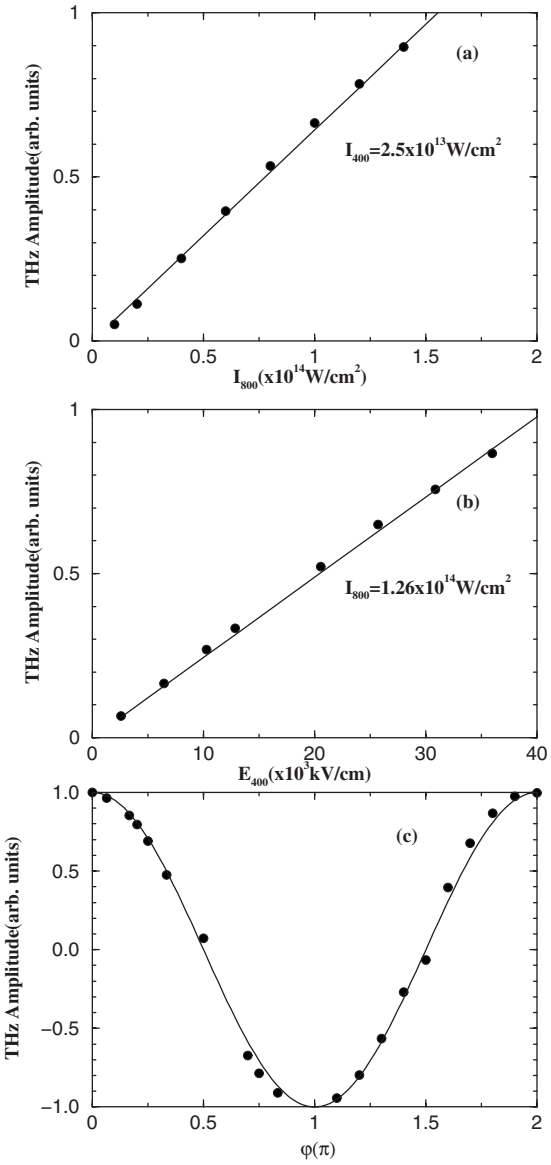


FIG. 13. Dependence of THz amplitude on (a) the intensity of the $\omega$ laser, (b) the amplitude of the $2\omega$ laser, and (c) the phase difference ($\varphi$) between the two lasers. The dots are the values calculated using the strong field approximation for the free-free transitions, and the solid lines are, respectively, the linear and cosine fittings to the corresponding dots.

variations in the THz strength relative to the parameters of the incident laser fields follow the same pattern.

## VI. OPTICAL BIASED POTENTIAL

The evidence above supports the notion that an atom can absorb one photon and emit two photons, one of which is in the THz frequency range, if the symmetry of the atom is broken. Unlike the FWM process, this three-photon process may be interpreted as a second-order nonlinearity that can produce a very large coefficient by itself [12,14,26]. This section discusses the simulation of this kind of process. The introduction of a spatially constant electric field $E_0$ is widely

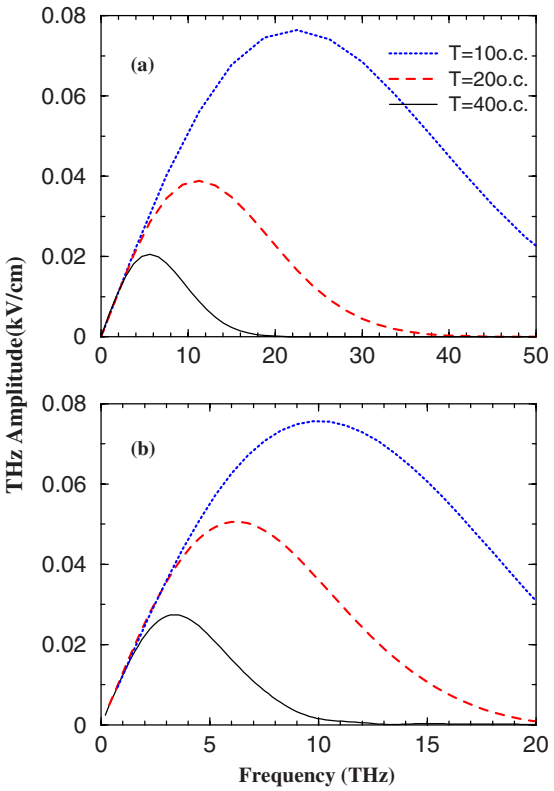


FIG. 14. (Color online) THz emissions upon mixing the fundamental and a long second harmonic laser fields. Durations of the fundamental laser field with 10 (dotted line), 20 (dashed line), and 40 o.c. (solid line) are adopted by using the methods of (a) strong field approximation and (b) solving TDSE for the short-range shallow potential model $V(x)=-0.3e^{-x^2/1.202}$. The intensities of the laser fields are the same as those in Fig. 9

used to break the system symmetry and enhance THz emissions. Equation (2) is replaced by

$$\hat{H}_I = -[\mathbf{E}_0 + \mathbf{E}f(t)\cos(\omega t)] \cdot \mathbf{r}. \tag{28}$$

When noble gases are used, it is possible to apply higher biased fields with an increased dielectric breakdown field of the gas by raising the absolute gas pressure. It is reported that the amplitude of the emitted THz field exhibits a linear relationship with the biased field strength and is almost independent of the absolute gas pressure [5]. This method is more often applied to semiconductors as the ionization potential is much lower and the system symmetry can be broken more easily. It has also been reported that electrons accelerated by a surface biased field result in an electric current that generates THz emissions with amplitudes demonstrating a linear relationship with the biased electric field [9–11]. Generally, biased electric fields in a range of 10–50 kV/cm can be applied for gases at normal pressures. In atomic systems, this value is negligible compared with the strength of nuclear electric field. So simulations are made for the short-range shallow potential model expressed by Eq. (18) with intensity of the fundamental 800 nm laser field to be $3.51 \times 10^{12}$ W/cm$^2$. The THz field amplitude demonstrates a linear relationship with the biased field as shown in Fig. 15(a).

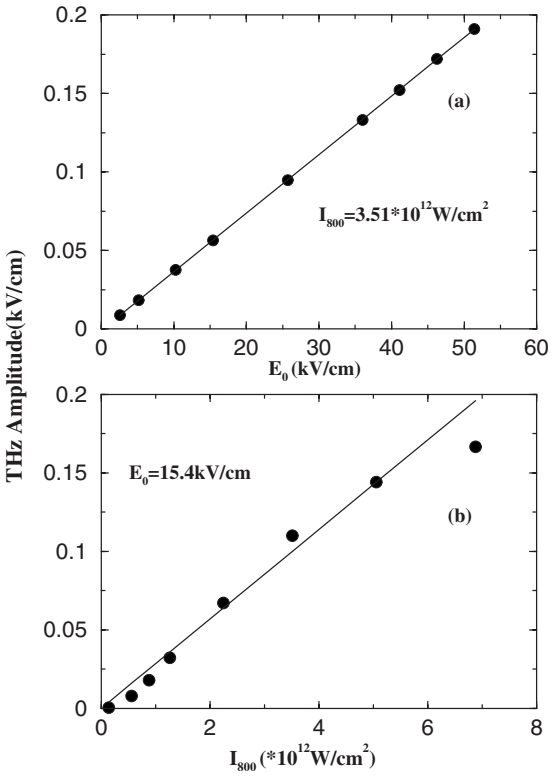


FIG. 15. Dependence of THz amplitude on (a) the magnitude of the spatially constant electric field $E_0$ and (b) the intensity of the fundamental laser field. The dots are the numerically calculated values for the short-range shallow potential model $V(x) = -0.3e^{-x^2/1.202}$ and the solid lines are their linear fittings.

Only three photons are involved in this THz emission process: two photons from the fundamental laser pulse and one photon of THz, so the amplitude of the THz fields is in proportion to the intensity of the laser pulse as shown in Fig. 15(b).

According to the four-photon THz emission process for the mixing of the fundamental and its second harmonic laser fields, the introduction of a field with THz frequency ($\omega_3$) also induces the second-order and other even-order harmonics. When two photons of the fundamental laser field are absorbed, a photon with $\hbar\omega_3$ of energy and a photon with a frequency of $2\omega-\omega_3$ located close to the second-order harmonic line are emitted as a result of applying a THz frequency laser field. Similarly, when the system absorbs two photons from the fundamental laser field and one THz photon, then a photon with a frequency of $2\omega+\omega_3$ is emitted. The corresponding peaks at $2\omega\pm\omega_3$ are evident in the emission spectrum. When the frequency of the incident field is low enough, its optical cycle is found to be longer than the duration time of the fundamental laser pulse. In this way, it acts like a spatial electrical field and the system symmetry is broken by the THz field. The emission spectrum around the second harmonics for $\omega_3$=5 THz=0.013 33$\omega$ depicted in the inset of Fig. 16(a) clearly shows the peaks at $2\omega\pm\omega_3$ and $2\omega$. Thus, both the three- and four-photon process models operate for the superposition of the fundamental and the THz frequency fields when $\omega_3$=0.013 33$\omega$. No matter which model is adopted to describe the physical process, the relationship of $E_{\mathrm{THz}} \propto \sqrt{I_{\omega_3} I_\omega}$ holds, as shown in Figs. 16(b) and 16(c). With a stronger THz field, the three peaks at $2\omega\pm\omega_3$ and $2\omega$ are all increased. The amplitudes of these peaks are also in proportion to the amplitude of the THz field in accordance with the THz emission generation mechanism. This relationship, in accordance with previous studies [56,57], is

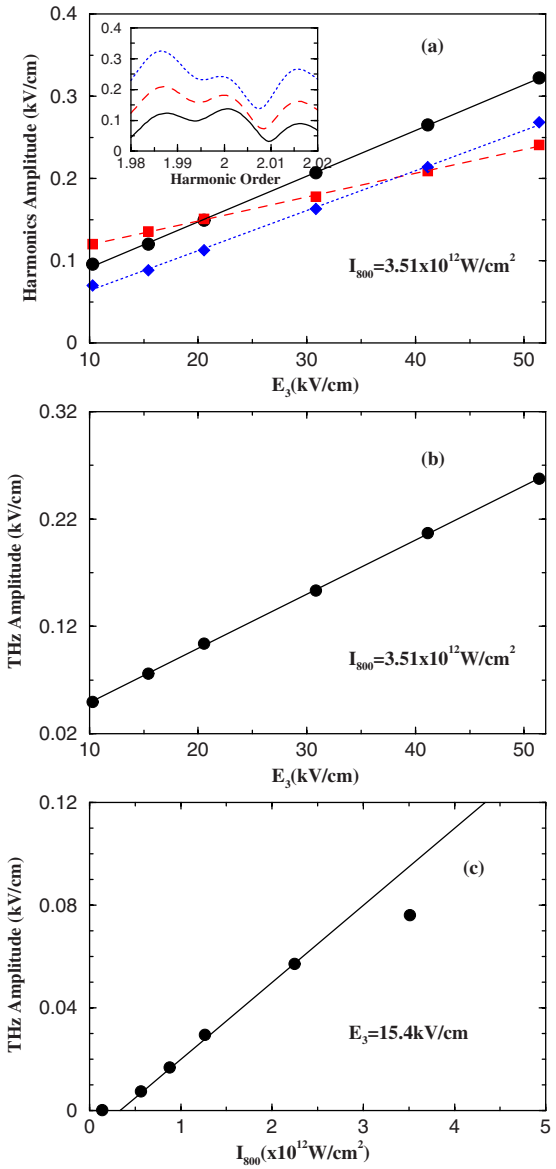


FIG. 16. (Color online) (a) Strength dependence of the three harmonics located at $2\omega-\omega_3$ (circle, solid line), $2\omega$ (square, dashed line), and $2\omega+\omega_3$ (diamond, dotted line) on the amplitude of the THz field for the mixing of the fundamental and a 5 THz frequency ($\omega_3$) fields. Emission spectra around the second harmonics are displayed in the inset. The intensity of the fundamental laser field is chosen to be $3.51\times10^{12}$ W/cm$^2$ and the amplitude of the THz field is chosen to be 15.42 Kv/cm (solid line), 30.84 kV/cm (dashed line), and 51.4 kV/cm (dotted line), respectively. Dependence of the emitted THz field amplitude on (b) the amplitude of the 5 THz field and (c) the intensity of the fundamental laser field is also shown. The lines are linear fittings to the dots of the numerically calculated data.

illustrated in Fig. 16(a) and supports the validity of the three-or four-photon process in describing THz generation.

## VII. CONCLUSION

In this study THz emissions from atoms in intense fs Gaussian-enveloped laser pulses are investigated by solving TDSE. It is first deduced from results with one-component laser fields that the excitations of electrons to continuum and high Rydberg states are essential for the generation of THz emissions. Transitions between the intermediate states lying above the ionization threshold of the atomic system are found to be much more effective for generating THz emissions than those states below the ionization threshold. This finding serves to enhance understanding of the behavior of an atom in intense laser fields since previous investigations often omit these continuum free-free transitions in the three-step model of HHG. Herein, an explanation based on multiphoton transition processes of how to substantially enhance THz emissions by mixing fundamental and second-order harmonic laser fields has been postulated. This mechanism, in light of a short-range shallow potential model, is shown to have all the usual low intensity four-photon mixing characteristics. In support of the TDSE predictions about the THz emission processes, an analytical strong field approximation is used to calculate the optical transition amplitudes between the continuum states. The results obtained from solving the TDSE and from the strong field approximation are found to be in accordance with the scaling law observed in previous studies. A biased electric field is also used to break the symmetry of the atomic system to facilitate the predominance of three-photon processes. This process enhances the THz emissions substantially and, consistent with previous studies, the dependence of the THz field strength on the applied electric fields is also predicted. Finally, a 5 THz frequency laser field is superposed on the fundamental laser field to induce the generation of second-order and other even-order harmonics as an inverse multiphoton process of the THz emissions discussed in the present study.

## ACKNOWLEDGMENTS

The authors are very grateful to Dr. Lesley Pereira, Central South University, Changsha, People's Republic of China for assistance in revising the paper extensively to improve the readability and presentation. This work was supported by the National Natural Science Foundation of China under Grant No. 10734140, the National Basic Research Program of China (973 Program) under Grant No. 2007CB815105, and the National High-Tech ICF Committee in China.

[1] Y. Chen, M. Yamaguchi, M. Wang, and X.-C. Zhang, Appl. Phys. Lett. **91**, 251116 (2007).
[2] D. J. Cook and R. M. Hochstrasser, Opt. Lett. **25**, 1210 (2000).
[3] M. Kress, T. Löffer, S. Eden, M. Thomson, and H. G. Roskos, Opt. Lett. **29**, 1120 (2004).
[4] K. Y. Kim, J. H. Glownia, A. J. Taylor, and G. Rodriguez, Opt. Express **15**, 4577 (2007).
[5] T. Löffler and H. G. Roskos, J. Appl. Phys. **91**, 2611 (2002).
[6] T. Bartel, P. Gaal, K. Reimann, M. Woerner, and T. Elsaesser, Opt. Lett. **30**, 2805 (2005).
[7] X. Xie, J. Dai, and X.-C. Zhang, Phys. Rev. Lett. **96**, 075005 (2006).
[8] A. Houard, Y. Liu, A. Mysyrowicz, and B. Leriche, Appl. Phys. Lett. **91**, 241105 (2007).
[9] M. Spasenović, M. Betz, L. Costa, and H. M. van Driel, Phys. Rev. B **77**, 085201 (2008).
[10] D. Wang, A. Zhang, L. Yang, and M. M. Dignam, Phys. Rev. B **77**, 115307 (2008).
[11] Y. C. Shen, P. C. Upadhya, E. H. Linfield, H. E. Beere, and A. G. Davies, Phys. Rev. B **69**, 235325 (2004).
[12] S. L. Chuang, S. Schmitt-Rink, B. I. Greene, P. N. Saeta, and A. F. J. Levi, Phys. Rev. Lett. **68**, 102 (1992).
[13] L. Yang, B. Rosam, K. Leo, and M. M. Dignam, Phys. Rev. B **72**, 115313 (2005).
[14] R. Atanasov, A. Haché, J. L. P. Hughes, H. M. van Driel, and J. E. Sipe, Phys. Rev. Lett. **76**, 1703 (1996).
[15] G. Meinert, L. Bányai, P. Gartner, and H. Haug, Phys. Rev. B **62**, 5003 (2000).
[16] A. Reklaitis, Phys. Rev. B **77**, 153309 (2008).
[17] Markus Kreß, Torsten Löffler, Mark D. Thomson, Reinhard Dörner, Hartmut Gimpel, Karl Zrost, Thorsten Ergler, Robert Moshammer, Uwe Morgner, Joachim Ullrich, and Hartmut G. Roskos, Nat. Phys. **2**, 327 (2006).
[18] X. C. Zhang, Y. Jin, T. D. Hewitt, T. Sangsiri, L. E. Kingsley, and M. Weiner, Appl. Phys. Lett. **62**, 2003 (1993).
[19] B. B. Hu, X. C. Zhang, and D. H. Auston, Phys. Rev. Lett. **67**, 2709 (1991).
[20] V. B. Gildenburg and N. V. Vvedenskii, Phys. Rev. Lett. **98**, 245002 (2007).
[21] R. Kersting, K. Unterrainer, G. Strasser, H. F. Kauffmann, and E. Gornik, Phys. Rev. Lett. **79**, 3038 (1997).
[22] K. Leo, J. Shah, E. O. Göbel, T. C. Damen, S. Schmitt-Rink, W. Schäfer, and K. Köhler, Phys. Rev. Lett. **66**, 201 (1991).
[23] H. G. Roskos, M. C. Nuss, J. Shah, K. Leo, D. A. B. Miller, A. M. Fox, S. Schmitt-Rink, and K. Köhler, Phys. Rev. Lett. **68**, 2216 (1992).
[24] X. C. Zhang, Y. Jin, and X. F. Ma, Appl. Phys. Lett. **61**, 2764 (1992).
[25] X. C. Zhang, X. F. Ma, Y. Jin, T. M. Lu, E. P. Boden, P. D. Phelps, K. R. Stewart, and C. P. Yakymyshyn, Appl. Phys. Lett. **61**, 3080 (1992).
[26] P. Y. Han, M. Tani, F. Pan, and X. C. Zhang, Opt. Lett. **25**, 675 (2000).
[27] D. Côté, N. Laman, and H. M. van Driel, Appl. Phys. Lett. **80**, 905 (2002).
[28] Q. Chen and X. C. Zhang, Appl. Phys. Lett. **74**, 3435 (1999).
[29] T. Löffler, F. Jacob, and H. G. Roskos, Appl. Phys. Lett. **77**, 453 (2000).
[30] H. Hamster, A. Sullivan, S. Gordon, W. White, and R. W.

Falcone, Phys. Rev. Lett. **71**, 2725 (1993).
[31] M. D. Feit, J. A. Fleck, Jr., and A. Steiger, J. Comput. Phys. **47**, 412 (1982).
[32] J. A. Fleck, Jr., J. R. Morris, and M. D. Feit, Appl. Phys. (Berlin) **10**, 129 (1976).
[33] K. Burnett, V. C. Reed, J. Cooper, and P. L. Knight, Phys. Rev. A **45**, 3347 (1992).
[34] Xiao-Min Tong and Shih-I Chu, Chem. Phys. **217**, 119 (1997).
[35] X. Chen, A. Sanpera, and K. Burnett, Phys. Rev. A **51**, 4824 (1995).
[36] J. L. Krause, K. J. Schafer, and K. C. Kulander, Phys. Rev. A **45**, 4998 (1992).
[37] M. R. Hermann and J. A. Fleck, Jr., Phys. Rev. A **38**, 6000 (1988).
[38] Q. Su and J. H. Eberly, Phys. Rev. A **44**, 5997 (1991).
[39] P. B. Corkum, Phys. Rev. Lett. **71**, 1994 (1993).
[40] X.-M. Tong and Shih-I Chu, Phys. Rev. A **61**, 021802(R) (2000).
[41] A. Houard, Y. Liu, B. Prade, and A. Mysyrowicz, Opt. Lett. **33**, 1195 (2008).
[42] A. Hache, J. E. Sipe, and H. M. van Driel, IEEE J. Quantum Electron. **34**, 1144 (1998).
[43] E. Dupont, P. B. Corkum, H. C. Liu, M. Buchanan, and Z. R. Wasilewski, Phys. Rev. Lett. **74**, 3596 (1995).
[44] M. Sheik-Bahae, Phys. Rev. B **60**, R11257 (1999).
[45] T. M. Fortier, P. A. Roos, D. J. Jones, S. T. Cundiff, R. D. R. Bhat, and J. E. Sipe, Phys. Rev. Lett. **92**, 147403 (2004).
[46] C. Figueira de Morisson Faria, D. B. Milošević, and G. G. Paulus, Phys. Rev. A **61**, 063415 (2000).
[47] P. C. Li, X. X. Zhou, C. Z. Dong, and S. F. Zhao, Acta. Phys. Sin. **53**, 750 (2004).
[48] C. Figueira de Morisson Faria, R. Kopold, W. Becker, and J. M. Rost, Phys. Rev. A **65**, 023404 (2002).
[49] N. Laman, A. I. Shkrebtii, J. E. Sipe, and H. M. van Driel, Appl. Phys. Lett. **75**, 2581 (1999).
[50] Huynh Thanh Duc, T. Meier, and S. W. Koch, Phys. Rev. Lett. **95**, 086606 (2005).
[51] J. S. Blakemore, J. Appl. Phys. **53**, R123 (1982).
[52] M. Lewenstein, Ph. Balcou, M. Yu. Ivanov, Anne L'Huillier, and P. B. Corkum, Phys. Rev. A **49**, 2117 (1994).
[53] B. Wang, X. Li, and P. Fu, J. Phys. B **31**, 1961 (1998).
[54] X. X. Zhou, X. M. Tong, Z. X. Zhao, and C. D. Lin, Phys. Rev. A **72**, 033412 (2005).
[55] H. G. Muller, P. H. Bucksbaum, D. W. Schumacher, and A. Zavriyev, J. Phys. B **23**, 2761 (1990).
[56] J. Dai, X. Xie, and X.-C. Zhang, Phys. Rev. Lett. **97**, 103903 (2006).
[57] D. J. Cook, J. X. Chen, E. A. Morlino, and R. M. Hochstrasser, Chem. Phys. Lett. **309**, 221 (1999).